The Cryosphere Discuss., 4, 2143–2167, 2010
www.the-cryosphere-discuss.net/4/2143/2010/
doi:10.5194/tcd-4-2143-2010

The Cryosphere Discussions

Assessment of glacier melt-model transferability: comparison of temperature-index and energy-balance models

A. H. MacDougall[1], B. A. Wheler[1,*], and G. E. Flowers[1]

[1]Department of Earth Sciences, Simon Fraser University, Burnaby, British Columbia, Canada
[*]now at: Wek'èezhìi Land and Water Board, Northwest Territories, Canada

Received: 14 September 2010 – Accepted: 6 October 2010 – Published: 20 October 2010

Correspondence to: G. E. Flowers (gflowers@sfu.ca)

Published by Copernicus Publications on behalf of the European Geosciences Union.

Abstract

Transferability of glacier melt models is necessary for reliable projections of melt over large glacierized regions and over long time-scales. The transferability of such models has been examined for individual model types, but inter-comparison has been hindered by the diversity of validation statistics used to quantify transferability. We apply four common types of melt models – the classical degree-day model, an enhanced temperature-index model, a simplified energy-balance model and a full energy-balance model – to two glaciers in the same small mountain range. The transferability of each model is examined in space and over two melt seasons. We find that the full energy balance model is consistently the most transferable, with deviations in estimated glacier-wide surface ablation of $\leqslant$35% when the model is forced with parameters derived from the other glacier and/or melt season. The other three models have deviations in glacier-wide surface ablation of $\geqslant$100% under the same forcings. In addition, we find that there is no simple relationship between model complexity and model transferability.

1 Introduction

Climate warming is expected to reduce the extent of the Earth's mountain glaciers and ice caps during the 21st century, raising eustatic sea level and diminishing fresh water resources (Lemke et al., 2007). Recently there have been attempts to project the magnitude of glacier loss using glacier melt models applied over large regions or globally (e.g. de Woul and Hock, 2005; Oerlemans et al., 2005; Raper and Braithwaite, 2006; Schneeberger et al., 2003). Such studies have produced a wide range of projected contributions of mountain glaciers and ice caps to 21st century sea-level rise, from 4 cm Sea Level Equivalent (SLE) (Raper and Braithwaite, 2006) to 36 cm SLE (Bahr et al., 2009), motivating a reexamination of the assumptions necessary to apply these models over large regions. Glacier melt models can be broadly divided into empirical models, which correlate melt to air temperature, and physically-based models which

TCD
4, 2143–2167, 2010

use energy-balance theory to solve for the energy available to melt snow or ice (e.g. Hock, 2003, 2005). Although melt-model transferability may not be universally possible (Hock, 2003; Hock et al., 2007), limited mass-balance data make it necessary to apply melt models to large regions without site-specific recalibration.

Several studies have previously investigated the transferability of glacier melt models at regional scales (e.g. Carenzo et al., 2009; MacDougall and Flowers, 2010; Shea et al., 2009). Each of these studies uses a different melt model and each finds certain conditions under which the authors consider the respective model to be transferable. However, direct comparison of previously published studies is complicated by the inconsistency of performance metrics authors use to evaluate model transferability. In an attempt assess the relative transferability of different model types, we apply the classical temperature-index model (Braun et al., 1993), the enhanced temperature-index model of Hock (1999), a simplified energy-balance model based on that of Oerlemans (2001), and the distributed energy-balance model of MacDougall and Flowers (2010) to two small glaciers in the Donjek Range of the St. Elias Mountains. We conduct a series of experiments to quantify the transferability of each model between our two study glaciers and across the 2008 and 2009 melt seasons. Because of the proximity of our study sites in space and the short duration of our data sets (two seasons), this assessment of transferability should be interpreted as an optimistic one.

1.1 Study site

The St. Elias Mountains, located in Northwestern North America, are characterized by extreme topographic gradients (Clarke and Holdsworth, 1984) and host one of the largest glacierized regions outside of the Arctic or Antarctic (Arendt et al., 2008). During the latter decades of the 20th century, glaciers in Southeastern Alaska and the Coast Mountains of Northwestern North America contributed more to sea-level rise than any other glacierized region (Kaser et al., 2006; Lemke et al., 2007). Within this region, the greatest single contribution came from the glaciers of the St. Elias Mountains (Berthier et al., 2010). The Donjek Range is located at the eastern edge

TCD
4, 2143–2167, 2010

of the St. Elias Mountains in the Southwestern Yukon Territory of Canada (Fig. 1a.). The range is separated from the Gulf of Alaska by less than 100 km, yet experiences a continental climate due to the orographic barriers between the range and the coast (L'Heureux et al., 2004).

This study is conducted on two unnamed mountain glaciers 10 km apart (Fig. 1b). The study glaciers are of similar size and are located on opposing sides of the range crest. One glacier has a predominantly southerly aspect and a surge-type dynamic regime (De Paoli and Flowers, 2009) and is henceforth referred to as "South Glacier" (Fig . 1c). The other has a northwesterly aspect and is referred to as "North Glacier" (Fig. 1d). South Glacier is thought to have a polythermal structure (De Paoli and Flowers, 2009) similar to that of Storglaciären in Northern Sweden (Pettersson et al., 2004). The thermal regime of North Glacier is also presumed to be polythermal but has not been studied. These glaciers were chosen as focussed study sites among the >20 mountain glaciers of the Donjek Range due to their geometric similarities and opposing aspects. The two glaciers have been studied in detail since 2007, with the full complement of instruments required for this study deployed in the 2008 and 2009 field seasons.

2 Methods

2.1 Field methods

2.1.1 Instrumentation and measurements

Parallel meteorological and mass-balance measurements were made on each glacier in 2008 and 2009. Automatic weather stations (AWSs) are located in the central ablation zones of each glacier at ~2300 m above sea level (a.s.l.). The AWSs are instrumented to measure typical meteorological variables, as well as net radiation, and incoming and reflected shortwave radiation (Table 1). An Ultra Sonic Depth Gauge

TCD
4, 2143–2167, 2010

(USDG), which measures surface lowering, is deployed several meters from each AWS. Summer and winter balance is measured at an array of 18 (17) ablation stakes deployed on South (North) Glacier (Fig. 1c,d). Snow-pits are excavated near the AWSs and in the accumulation zones of the glaciers each May, in order to evaluate the density and structure of the snowpack.

2.1.2 Data processing

Meteorological data are gap-filled using linear interpolation. No gap in the 2007–2009 record is longer than 30 min for deployed and undamaged instruments (see MacDougall and Flowers (2010) for details). The USDG record is used to estimate the time and magnitude of snowfall events, and based on measurments fresh snow is assumed to have a density of 200 kg m^{-3}. The ablation stake measurements are used to estimate mass balance following the method of Østrem and Brugman (1991). Initial snow-depth across the glacier is calculated by interpolating measured May snow-depths from the ablation stake locations to all grid points using linear regressions on slope and elevation for South Glacier, and linear regression on elevation for North Glacier (Wheler, 2009; MacDougall, 2010). Snowfall events at the AWS are extrapolated to the rest of the glacier using an empirical precipitation lapse rate (Table 2), a temperature melt/freeze threshold of 1 °C, and the rainfall records from the AWS.

2.2 Modelling methods

Four melt models are used to examine the relationship between model transferability and model complexity: (1) the Classical Temperature-Index Model (CTIM) (Braun et al., 1993); (2) the Enhanced Temperature-Index Model of Hock (1999) (ETIM); (3) a Simplified Energy-Balance Model based on that of Oerlemans (2001) (SEBM); (4) the Distributed Energy-Balance Model of MacDougall and Flowers (2010) (DEBM). This suite of models is similar to that used by Hock et al. (2007) to inter-compare the simulated long-term mass-balance of Storglaciären. We have omitted the enhanced

TCD
4, 2143–2167, 2010

temperature-index model of Pellicciotti et al. (2005) from this study, as it is designed to be tuned with the output of an energy balance model rather than with observations directly. Such tuning would present a methodological inconsistency for the purposes of our model inter-comparison study.

2.2.1 Classical temperature-index model (CTIM)

The CTIM is the simplest melt model considered and correlates temperature to melt with an empirical degree-day factor. As for most other implementations of this model, different degree-day factors are used for ice and snow (e.g. Braun et al., 1993). The model takes the form:

$$M = \begin{cases} \mathrm{DDF}_{\mathrm{snow/ice}} T_\mathrm{a} : T_\mathrm{a} > 0 \\ 0 : T_\mathrm{a} \leq 0 \end{cases} \quad (1)$$

where $\mathrm{DDF}_{\mathrm{snow/ice}}$ is the degree-day factor for snow or ice. The CTIM is driven with air temperature T_a and snowfall.

2.2.2 Enhanced temperature-index model (ETIM)

The ETIM is an extension of the classical temperature-index model, where both temperature and potential shortwave radiation are correlated to melt. Firn is treated as snow in the model by assigning an arbitrarily deep snow depth above the firn line (Hock, 1999). This model has been widely used and exhibits significant improvements in model skill over the clasical temperature-index approach, with a minimal increase in data requirements (e.g. Hock, 1999; Huss et al., 2008). The model takes the form:

$$M = \begin{cases} \left(\mathrm{MF} + r_{\mathrm{snow/ice}} I_\mathrm{p}\right) T_\mathrm{a} : T_\mathrm{a} > 0 \\ 0 : T_\mathrm{a} \leq 0 \end{cases} \quad (2)$$

where M is melt rate, MF is a temperature melt factor, $r_{\mathrm{snow/ice}}$ is the radiation melt factor for snow or ice, and I_p is the potential shortwave radiation. I_p varies in time and

TCD
4, 2143–2167, 2010

space due to the combined effects of the position of the sun and surface slope, surface aspect, and shading from the surrounding topography. The model is driven with air temperature and snowfall.

2.2.3 Simplified energy-balance model (SEBM)

The the simplified energy-balance model of Oerlemans (2001) takes the form:

$$Q_M = (S_{in}(1-\alpha)) + C_0 + C_1 T_a, \quad (3)$$

where T_a is air temperature, C_0 and C_1 are empirical factors that together take into account net longwave radiation and the turbulent heat fluxes. The incoming shortwave radiation (S_{in}) and albedo (α) are treated in an identical fashion as in the DEBM described below. The SEBM differs from the original simplified energy-balance model of Oerlemans (2001) only in its treatment of albedo. The model is driven with air temperature, incoming shortwave radiation, and snowfall.

2.2.4 Distributed energy-balance melt model (DEBM)

Energy-balance models parameterize or utilize measurements of all of the components of the surface energy balance of ice or snow to solve for the energy available for melt as a residual. Distributed energy-balance models extrapolate the surface energy balance across a grid on the glacier surface. A full description of the DEBM and model validation is given in MacDougall and Flowers (2010). A brief description of the model is recalled below.

The energy balance is written as:

$$Q_M = (S_{in}(1-\alpha) + L_{in} - L_{out}) + Q_H + Q_L - Q_g, \quad (4)$$

where S_{in} is incoming shortwave radiation, α is the albedo of the ice or snow surface, L_{in} is the incoming longwave radiation and L_{out} is the outgoing longwave radiation. Q_H

TCD
4, 2143–2167, 2010

is the sensible heat flux, the energy exchanged between the glacier and the atmosphere. Q_L is the latent heat flux, the heat transferred to or from the glacier through sublimation, deposition, evaporation or condensation. Q_g is the heat transferred to and from the glacier subsurface when the subsurface changes temperature. Q_M is the energy available to melt ice or snow. The sensible heat flux from rain was found to be negligible and is therefore disregarded.

To extrapolate measured incoming shortwave radiation (S_{in}) to each grid point, S_{in} is broken into direct and diffuse components following Collares-Pereira and Rabl (1979) and Hock and Holmgren (2005). Direct shortwave radiation is only incident on the fraction of the glacier unshaded by surrounded terrain, while diffuse radiation is assumed to originate from all parts of the sky equally and is therefore applied to all grid cells. If the AWS is shaded by surrounding topography all measured incoming shortwave radiation is diffuse (Hock and Holmgren, 2005); in this situation the ratio of direct to diffuse shortwave radiation from the most recent time where the AWS was unshaded is used to approximate direct shortwave radiation at unshaded grid cells.

Albedo (α), is parameterized following Hock and Holmgren (2005):

$$\alpha_t = \begin{cases} \alpha_{t-1} - a_1(\ln(T_a+1))e^{(a_2\sqrt{n_d})} & \text{if } n_d > 0 \text{ and } T_a > 0 \\ \alpha_{t-1} - a_3 e^{(a_2\sqrt{n_d})} & \text{if } n_d > 0 \text{ and } T_a < 0 \\ \alpha_{t-1} + a_4 P_s & \text{if } n_d = 0 \end{cases} \quad (5)$$

where α_{t-1} is the albedo at the previous time step, α_t is the albedo at the current time step, n_d is the number of days since the last snow fall, P_s is the measured rate of snow fall, T_a is air temperature and $a_{1:4}$ are constants that must be found through calibration (Hock and Holmgren, 2005). A constant elevation firn-line was assigned based on field observations (Table 2). Ice is assumed to have a constant albedo (e.g. Hock and Holmgren, 2005; Oerlemans and Knap, 1998).

Outgoing longwave radiation (L_{out}) is calculated from the temperature of the ice or snow surface (T_s) according to the Stefan-Boltzmann relationship. The surface temperature (T_s) and the subsurface heat flux (Q_g) are calculated using a simple subsurface

TCD
4, 2143–2167, 2010

scheme, in which Q_g is taken as the residual of the energy balance when it is negative. The subsurface flux is then forced into a thin subsurface layer such that

$$\Delta T_s = \frac{Q_g}{\rho_s c_s h} \Delta t\,, \tag{6}$$

where Δt is the model time-step in seconds, ρ_s is the surface material density, c_s is the specific heat capacity of ice, and h is the thickness of the subsurface layer. This subsurface scheme is a compromise between a more complicated multi-layer subsurface model and simpler constant temperature or iterative approximations. The scheme allows for temporary heat storage in the subsurface with minimal data requirements (Wheler and Flowers, 2010). Incoming longwave radiation (L_{in}) is computed as the residual of the radiative energy balance at the AWS location and is assumed to be constant over the entire glacier, following Hock and Holmgren (2005).

Sensible (Q_H) and latent heat fluxes (Q_L) are calculated using the bulk aerodynamic approach as in other recent DEBM studies (e.g. Anderson et al., 2010; Anslow et al., 2008; Brock et al., 2000; Hock and Holmgren, 2005). The aerodynamic roughness-length (z_o) used in the bulk aerodynamic approach is estimated using the snow aerodynamic roughness length evolution parameterization of Brock et al. (2006):

$$\ln(z_o) = b_1 \left(\arctan \left[\frac{(P_{dd} - b_2)}{b_3} \right] \right) - b_4\,, \tag{7}$$

where P_{dd} is the base 10 logarithm of the sum of daily maximum temperatures since the last snow fall event and $b_{1:4}$ are empirical constants. We use the mean value of the measured roughness of ice for each glacier. Firn is treated simply as very old snow by setting P_{dd} to be arbitrarily large. The DEBM is driven by air temperature, incoming shortwave radiation, net radiation, relative humidity, barometric pressure, snowfall, and wind speed records from the AWS.

TCD
4, 2143–2167, 2010

2.2.5 Model calibration and tuning

The three models with empirical melt factors (CTIM, ETIM and SEBM) are tuned by minimizing the root mean square error (RMSE) between measured and modelled ablation at the stake locations. The DEBM is calibrated using the record of albedo at the AWSs to solve for albedo parameters separately for each glacier and for each summer. The snow roughness-length evolution parameters are calibrated to roughness-length measurements that were taken only in the summer of 2009. The roughness-length measurements from both glaciers were used together for the calibration, as insufficient data exist to calibrate independently for each glacier. The mass-balance data are not used to calibrate the DEBM. See MacDougall and Flowers (2010) for details. The albedo parameterization for the SEBM is calibrated in an identical fashion to that for the DEBM.

2.3 Model transferability experiment design

To evaluate relative model skill, control runs were performed in which each model was run for each glacier and year using locally derived parameter values. Control runs are also used a reference against which to evaluate the results of the transferability tests.

Model transferability is the ability of a model calibrated for one time and location to produce realistic results for another time and/or location. Here we describe transferability in terms of model parameter values: that is, the ability of parameters calibrated for one time or location to describe another. We assess parameter transferability in time, in space and in space and time together for each model (Fig. 2). In each of these tests the parameter values derived for one glacier and year are used in place of those locally derived for the other glacier and/or year. We use the RMSE between the simulated and the measured cumulative ablation at the stake locations to evaluate the success of the model transfer. An additional experiment is carried out to test the robustness of the DEBM transfers, wherein the albedo parameterization for the DEBM is replaced with the albedo parameterization of Oerlemans and Knap (1998). The implications of this experiment will be explored in the discussion section.

TCD
4, 2143–2167, 2010

3 Results

3.1 Comparison to ablation stakes

The RMSE values for the control runs relative to the ablation stake measurements are shown in Fig. 3 for each model and data set (○ symbol). For both glaciers the model with the highest model skill is the ETIM for the 2008 simulations and the SEBM for the 2009 simulations. The lowest model skill is achieved by the SEBM for both glaciers in 2008, the CTIM for South Glacier 2009, and the DEBM for North Glacier 2009.

In 11 of 16 temporal transferability tests (× symbol in Fig. 3) the results more closely resemble the control runs than do those of any of the other transferability tests. This is particularly true for the DEBM (see DEBM in Fig. 3), where all of the temporal transferability tests are close to the control run, though untrue for the SEBM where none of the temporal transferability tests are closest to the control. There is a high variability in the results from spatial and spatial-temporal model transfer tests (□ and ◊ symbols, respectively in Fig. 3) but these transfers frequently produce much larger errors than the control runs.

The comparison between model results in Fig. 3 demonstrates that the DEBM is the most transferable of the models considered, as assessed by the spread of transferability test results. The SEBM is the second most transferable model for the North Glacier 2009 experiments, yet the least transferable for the North Glacier 2008 experiment. The ETIM performs better than the CTIM, but more poorly than the DEBM in each experiment. The only exceptions to the DEBM exhibiting the highest transferability are: the spatial transfer on North Glacier in 2008, where all of the models achieve similar RMSEs, the spatial-temporal transfer on South Glacier in 2008 where the SEBM performs best, and the spatial transfer on South Glacier in 2009 where the SEBM performs better than all of the other models.

TCD
4, 2143–2167, 2010

3.2 Comparison between control runs

Glacier melt models are typically applied beyond the stake locations to estimate surface ablation for an entire glacierized basin. Such estimates are shown for each of the control runs in Fig. 4. The spatial patterns of surface ablation in Fig. 4 testify to the increasing complexity of model output with increasing model sophistication. The more complex models estimate higher glacier-wide surface ablation (A_s) than the simpler models. The difference between the highest and lowest estimates of A_s for each glacier and year are considerable, ranging between 24% and 41% of the value of A_s estimated by the DEBM. This large variability is disconcerting, as each of these modelled values of ablation can justifiably be considered a valid estimate.

3.3 Comparison of transfer experiments to control runs

The absolute deviations between values of A_s estimated in each transfer test and estimated in the control run for a given model (Fig. 5) clearly demonstrate that only the DEBM transfer tests consistently produce estimated ablation anywhere close to the control run. The greatest deviation for the CTIM is 0.66 m w.e. (137% relative to control run A_s), for the ETIM 0.50 m w.e. (100%), for the SEBM 0.58 m w.e. (185%), and for the DEBM 0.16 m w.e. (35%). The spatial distributions of the difference in estimated surface ablation between the control run and each spatial-temporal transferability test for a given model are shown in Fig. 6. This figure demonstrates that the differences are proportional to the magnitude of ablation for the empirical models (CTIM and ETIM), while more complex difference patterns arise for the energy-balance models (SEBM and DEBM). Similar patterns are found for the individual temporal transfer and spatial transfer experiments (not shown).

TCD
4, 2143–2167, 2010

4 Discussion

The outcome that a physically-based glacier melt model is more transferable than empirical models is not a surprise (Hock, 2005). A model that better describes a physical system is expected to be more transferable than one that lumps site-specific properties and weather conditions together (Hock, 2005). This intuitive result has however, to our knowledge, not been previously demonstrated beyond a single glacier study site.

An intriguing outcome of these experiments is that, aside from the DEBM being more transferable than the other models, there is no simple relationship between model complexity and transferability. The relatively low transferability of the SEBM is surprising considering that the highest model sensitivity in the DEBM comes from the albedo parameterization (MacDougall and Flowers, 2010), which is treated in an identical fashion in the SEBM. This suggests that the SEBM's transferability is affected by the model's treatment of the turbulent and longwave heat fluxes, despite these fluxes generally being of secondary importance in our study area (MacDougall and Flowers, 2010).

Unlike the other models considered here, the DEBM has many subcomponents that may differ from those found in other full energy balance models (Brock et al., 2000; Anslow et al., 2008; Hock and Holmgren, 2005; Anderson et al., 2010, e.g.). It is therefore valid to ask whether the high model transferability found in these experiments is unique to the DEBM or its application here, rather than being a general result for all energy balance models of similar or greater complexity. To investigate this question the most sensitive component of the DEBM, the albedo evolution parameterization, was substituted and the transferability experiments repeated. The substitute albedo parameterization was that of Oerlemans and Knap (1998) which relates the albedo of snow to the snow depth and the time elapsed since the last snowfall. Firn and ice have constant albedos. The results of these tests (Fig. 3, DEBM-OK) demonstrate, with one exception, that the transferability tests are robust to the albedo substitution. This outcome supports the hypothesis that the high DEBM transferability is a property of full energy-balance models, rather than being unique to our experiments. That said, the

TCD
4, 2143–2167, 2010

choice of parameterizations is still important as results do not always follow the general pattern expected of the models.

5 Conclusions

We examined the transferability in space and time of four commonly used types of glacier melt models applied to two small glaciers in the St. Elias Mountains of Northwestern Canada. Our results demonstrate that the physically-based energy-balance model is the most transferable model in space and time, exhibiting ⩽35% variation in estimated glacier-wide surface ablation when using model parameters calibrated for a different melt season and/or another nearby glacier. Under the same conditions, the other models produced variations in estimated glacier-wide surface ablation exceeding 100%. No simple relationship between model complexity and model transferability is observed. Deviations in estimated glacier-wide surface ablation between the models in the control runs themselves were 24–41%. These results suggest that physically-based models should be the first choice when applying a glacier melt model over large regions. If insufficient data exist to implement such models, enhanced temperature-index models appear to be the next most appropriate choice. There is a need for similar experiments to be conducted in other glacierized regions and over longer time scales for a general confirmation of the conclusions presented here.

Acknowledgements. We are grateful to the Natural Science and Engineering Research Council of Canada (NSERC), the Canada Foundation of Innovation (CFI), the Canada Research Chairs (CRC) program, the Northern Scientific Training Program (NSTP), and Simon Fraser University for funding. AHMD is grateful for his support from NSERC PGS-M. Permission to conduct this research was granted by the Kluane First Nation, Parks Canada, and the Yukon Territorial Government. Support from the Kluane Lake Research Station (KLRS) and Kluane National Park and Reserve is greatly appreciated. We are indebted to Andy Williams, Sian Williams, Lance Goodwin (KLRS), Doug Makkonen and Stephen Soubliere (Trans North Helicopters) for logistical support, and to P. Belliveau, G. Rosenkjær, N. Roux, A. Jarosch, L. Mingo, J. Logher, F. Anslow, C. Schoof, S. Heðinsdóttir, and A. Rushmere for field assistance.

TCD
4, 2143–2167, 2010

References

Anderson, B., MacKintosh, A., Stumm, D., George, L., Kerr, T., Winter-Billington, A., and Fitzsimons, S.: Climate sensitivity of a high-precipitation glacier in New Zealand, J. Glaciol., 56, 114–128, 2010. 2151, 2155

Anslow, F., Hostetler, S., Bidlake, W. R., and Clark, P. U.: Distributed energy balance modelling of South Cascade Glacier, Washington and assessment of model uncertainty, J. Geophys. Res., 113, doi:10.1029/2007JF000850, 2008. 2151, 2155

Arendt, A., Luthcke, S., Larsen, C., Abdalati, W., Krabill, W., and Beedle, M.: Validation of high-resolution GRACE mascon estimates of glacier mass changes in the St. Elias Mountains, Alaska, USA, using aircraft laser altimetry, J. Glaciol., 256, 165–172, 2008. 2145

Bahr, D., Dyurgerov, M., and Meier, M.: Sea-level rise from glaciers and ice caps: a lower bound, Geophys. Res. Lett., 36, doi:10.1029/2008GL036309, 2009. 2144

Berthier, E., Schiefer, E., Clarke, G., Menounos, B., and Rémy, F.: Contribution of Alaskan glaciers to sea-level rise derived from satellite imagery, Nat. Geosci., 3(2), 92–95, doi:10.1038/NGEO737, 2010. 2145

Braun, L., Grabs, W., and Rana, B.: Application of a conceptual precipitation-runoff model in the Langtang Khola Basin, Nepal Himalaya, in: Snow and Glacier Hydrology, Proceedings of the Kathmandu Symposium 1992, edited by: Young, G., 221–237, IAHS, Wallingford, England OX10 8BB, 1993. 2145, 2147, 2148

Brock, B., Willis, I., and Sharp, M. J.: Measurement and parameterization of albedo variations at Haut Glacier d'Arolla, Switzerland, J. Glaciol., 46, 657–688, doi:10.3189/172756500781832675, 2000. 2151, 2155

Brock, B., Willis, I. C., and Sharp, M. J.: Measurement and parameterization of aerodynamic roughness length at Haut Glacier d'Arolla, Switzerland, J. Glaciol., 52, 281–297, 2006. 2151

Carenzo, M., Pellicciotti, F., Rimkus, S., and Burlando, P.: Assessing the transferability and robustness of an enhanced temperature-index glacier-melt model, J. Glaciol., 55, 258–274, 2009. 2145

Clarke, G. and Holdsworth, G.: Glaciers of the St. Elias Mountains, US Geological Survey professional paper, Washington, DC, USA, ISSN 1044-9612, 1984. 2145

Collares-Pereira, M. and Rabl, A.: The average distribution of solar radiation: correlations between daily and hourly insolation values, Sol. Energy, 22, 155–164, 1979. 2150

De Paoli, L. and Flowers, G.: Dynamics of a small surge-type glacier using one-dimensional

TCD
4, 2143–2167, 2010

geophysical inversion, J. Glaciol., 55, 1101–1112, 2009. 2146
de Woul, M. and Hock, R.: Static mass-balance sensitivity of Arctic glaciers and ice caps using a degree day approach, Ann. Glaciol., 42, 217–224, 2005. 2144
Hock, R.: A distributed temperature-index ice- and snowmelt model including potential direct solar radiation, J. Glaciol., 45(149), 101–111, 1999. 2145, 2147, 2148
Hock, R.: Temperature index melt modelling in mountain areas, J. Hydrol., 282, 104–115, 2003. 2145
Hock, R.: Glacier melt: a review of processes and their modelling, Prog. Phys. Geog., 29(3), 362–391, 2005. 2145, 2155
Hock, R. and Holmgren, B.: A distributed energy-balance model for complex topography and its application to Storglaciären, Sweden, J. Glaciol., 51, 25–36, doi:10.3189/172756505781829566, 2005. 2150, 2151, 2155
Hock, R., Radić, V., and de Woul, M.: Climate sensitivity of Storglaciären, Sweden: an intercomparison of mass-balance models using ERA-40 re-analysis and regional climate model data, Ann. Glaciol., 46, 342–348, 2007. 2145, 2147
Huss, M., Farinotti, D., Bauder, A., and Funk, M.: Modelling runoff from highly glacierized alpine drainage basins in a changing climate, Hydrol. Process., 22, 3888–3902, 2008. 2148
Kaser, G., Cogley, J., Dyurgerov, M., Meier, M., and Ohmura, A.: Mass balance of glaciers and ice caps: Consensus estimates for 1961–2004, Geophys. Res. Lett., 33, doi:10.1029/2006GL027511, 2006. 2145
Lemke, P., Ren, J., Alley, R., Allison, I., Carrasco, J., Flato, G., Fujii, Y., Kaser, G., Mote, P., Thomas, R., and Zhang, T.: Observations: changes in snow, ice and frozen ground, in: Climate Change 2007: The Physical Science Basis. Contribution of Working Group I to the Fourth Assessment Report of the Intergovernmental Panel on Climate Change, edited by: Solomon, S., Qin, D., Manning, M., Chen, Z., Marquis, M., Averyt, K., Tignor, M., and Miller, H., Cambridge University Press, Washington, DC, USA, 2007. 2144, 2145
L'Heureux, M., Mann, M., Cook, B., Gleason, B., and Voss, R.: Atmospheric circulation influences on seasonal precipitation patterns in Alaska during the latter 20th century, J. Geophys. Res., 109, doi:10.1029/2003JD003845, 2004. 2146
MacDougall, A.: Distributed energy-balance glacier melt-modelling in the Donjek Range of the St. Elias Mountains, Yukon Territory, Canada: model transferability in space and time, Master's thesis, Simon Fraser University, Burnaby, British Columbia, Canada, in preparation, 2010. 2147

TCD
4, 2143–2167, 2010

MacDougall, A. and Flowers, G.: Spatial and temporal transferability of a distributed energy-blance glacier melt-model, submitted, J. Climate, 2010. 2145, 2147, 2149, 2152, 2155
Oerlemans, J.: Glaciers and Climate Change, 1st edn., Swets and Zeitlinger BV, Lisse, 2001. 2145, 2147, 2149
Oerlemans, J. and Knap, W. H.: A one year record of global radiation and albedo in the ablation zone of Morteratschgletscher, Switzerland,, J. Glaciol., 44, 231–238, 1998. 2150, 2152, 2155, 2164
Oerlemans, J., Bassford, R., Chapman, W., Dowdeswell, J., Glazovsky, A., Hagen, J., Melvold, K., de Ruyter de Wildt, M., and van de Wal, R.: Estimating the contribution of Arctic glaciers to sea-level change in the next 100 years, Ann. Glaciol., 42, 230–236, 2005. 2144
Østrem, G. and Brugman, M.: Glacier mass-balance measurements: a manual for field and office work, National Hydrology Research Institute, Saskatoon Canada, 1991. 2147
Pellicciotti, F., Brock, B., Strasser, U., Burlando, P., Funk, M., and Corripio, J.: An enhanced temperature-index glacier melt model including the shortwave radiation balance: development and testing for Haut Glacier d'Arolla, Switzerland, J. Glaciol., 51, 573–587, 2005. 2148
Pettersson, R., Jansson, P., and Blatter, H.: Spatial variability in water content at the cold–temperate transition surface of the polythermal Storglaciären, Sweden, J. Geophys. Res., 109, doi:10.1029/2003JF000110, 2004. 2146
Raper, S. and Braithwaite, R.: Low sea level rise projections from mountain glaciers and ice-caps under global warming, Nature, 439, 311–313, 2006. 2144
Schneeberger, C., Blatter, H., Abe-Ouchi, A., and Wild, M.: Modelling changes in the mass balance of glaciers of the Northern Hemisphere for a transient 2 $\times CO_2$ scenario, J. Hydrol., 282, 145–263, 2003. 2144
Shea, J., Moore, R., and Stahl, K.: Derivation of melt factors from glacier mass-balance records in Western Canada, J. Glaciol., 55, 123–130, 2009. 2145
Wheler, B.: Glacier melt modelling in the Donjek Range, St. Elias Mountains, Yukon Territory, Master's thesis, Simon Fraser University, Burnaby, British Columbia, Canada, 2009. 2147
Wheler, B. and Flowers, G.: Glacier subsurface heat-flux characterizations for energy balance modelling in the Donjek Range, Southwest Yukon Territory, Canada, accepted, J. Glaciol., 2010. 2151

TCD
4, 2143–2167, 2010

Table 1. Instrumentation deployed at AWS locations on North Glacier and South Glacier. Instrument precision is taken from manufacturer's documentation. Rainfall for South Glacier was measured 500 m from AWS.

Variable	Instrument	Precision
Air temperature	HMP45C212 TRH Probe	±0.28°C
Relative humidity	HMP45C212 TRH Probe	±4%
Wind speed	RM Young 05103-10	±3 m s^{-1}
Wind direction	RM Young 05103-10	±3°
Surface height (distance)	SR50 Sonic Ranger	±0.4%
Net radiation	Kipp and Zonen NR-LITE	±5%
Barometric pressure	RM Young 61205V	±0.5 hPa
Shortwave radiation	Kipp and Zonen CMA6	±3%
Rainfall rate	TE525 Tipping Bucket Rain Gauge	0 to −3%

TCD
4, 2143–2167, 2010

Table 2. Parameters used in each of the four melt models. S08 is South Glacier 2008, S09 is South Glacier 2009, N08 is North Glacier 2008 and N09 is North Glacier 2009.

Symbol	Units	Description	S08	S09	N08	N09
All Models						
E_f	m	Firn line elevation	2450	2450	2400	2480
CTIM						
DDF_{snow}	w.e. mm d^{-1} K^{-1}	Degree day factor snow	7.0	6.0	2.5	5.0
DDF_{ice}	w.e. mm d^{-1} K^{-1}	Degree day factor ice	10.5	7.5	4.0	4.5
ETIM						
MF	w.e. mm d^{-1} K^{-1}	Temperature melt factor	2.0	1.9	1.4	1.7
r_{snow}	w.e. m h^{-1} K^{-1} W^{-1} μm^2	Radiation melt factor snow	0.66	0.62	0.23	0.46
r_{ice}	w.e. μm h^{-1} K^{-1} W^{-1} m^2	Radiation melt factor ice	1.5	1.05	0.56	0.72
SEBM						
C_0	W m^{-2}	Independent radiation constant	−49	−44	−57	−42
C_1	W m^{-2} K^{-1}	Temperature radiation constant	−2.2	2.8	1.8	3.9
SEBM and DEBM						
α_o	–	Initial albedo of snow	0.85	0.85	0.85	0.85
$\frac{d\alpha_i}{dZ}$	100 m^{-1}	Change in ice albedo with elevation	0.11	0.11	0	0
a_1	ln(°C)$^{-1}$	Albedo rate constant	0.032	0.031	0.042	0.030
a_2	day$^{-\frac{1}{2}}$	Albedo rate constant	−1.54	−1.68	−1.71	−1.61
a_3	–	Albedo rate constant	0.0074	0.0112	0.0104	0.0142
a_4	h m^{-1}	Albedo rate constant	44	30	88	60
α_i	–	Albedo of ice	0.34	0.33	0.44	0.43
α_{slim}	–	Lower limit of snow albedo	0.66	0.66	0.66	0.66
α_{flim}	–	Lower limit of firn albedo	0.56	0.56	0.56	0.56
α_{stof}	–	Albedo snow–firn transition	0.03	0.03	0.03	0.03
α_{ilim}	–	Lower limit of ice albedo	0.16	0.16	0.27	0.27
Γ_T	K km^{-1}	Temperature lapse rate	−6.0	−6.0	−5.3	−5.3
Γ_p	mm km^{-1}	Precipitation lapse rate	2.3	2.3	1.2	1.2
DEBM						
α_{ter}	–	Albedo of terrain	0.21	0.21	0.21	0.21
ϵ_{ter}	–	Emissivity of terrain	0.95	0.95	0.95	0.95
T_{sub}	°C	Min subsurface temperature	−30	−30	−30	−30
h	m	Thickness of subsurface	0.10	0.10	0.10	0.10
Z_{thr}	m	Snow threshold	0.01	0.01	0.01	0.01
b_1	mm	Roughness rate constant	0.91	0.91	0.91	0.91
b_2	°C	Roughness rate constant	1.36	1.36	1.36	1.36
b_3	°C	Roughness rate constant	0.054	0.054	0.054	0.054
b_4	mm	Roughness rate constant	2.3	2.3	2.3	2.3
z_{oi}	mm	Roughness length of ice	0.65	0.65	0.20	0.20

TCD
4, 2143–2167, 2010

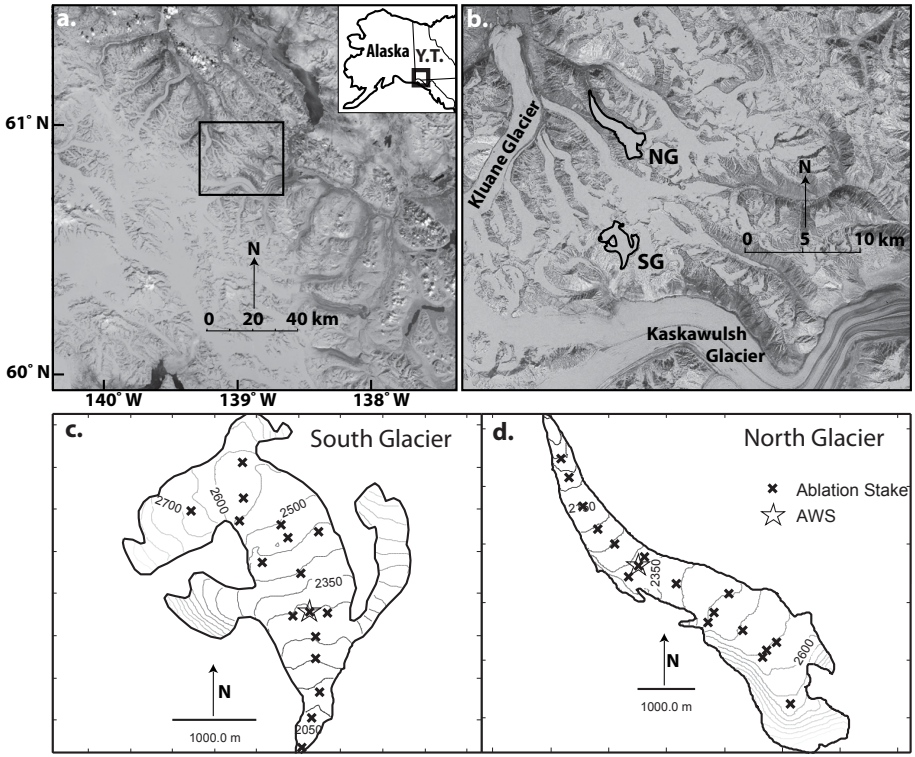

Fig. 1. Map of study region. **(a)** St. Elias Mountains in Southwest Yukon Territory, Canada (inset). Donjek Range study area is shown in the box. Images provided through NASA's Scientific Data Purchase Project and under NASA contract by Earth Satellite Corporation. **(b)** Donjek Range study area between the Kluane and Kaskawulsh Glaciers. Study glaciers are outlined and labeled: "NG" for North Glacier, "SG" for South Glacier. **(c)** Surface contour map of South Glacier with locations of ablation stakes and AWS. **(d)** As for (c) but for North Glacier.

TCD
4, 2143–2167, 2010

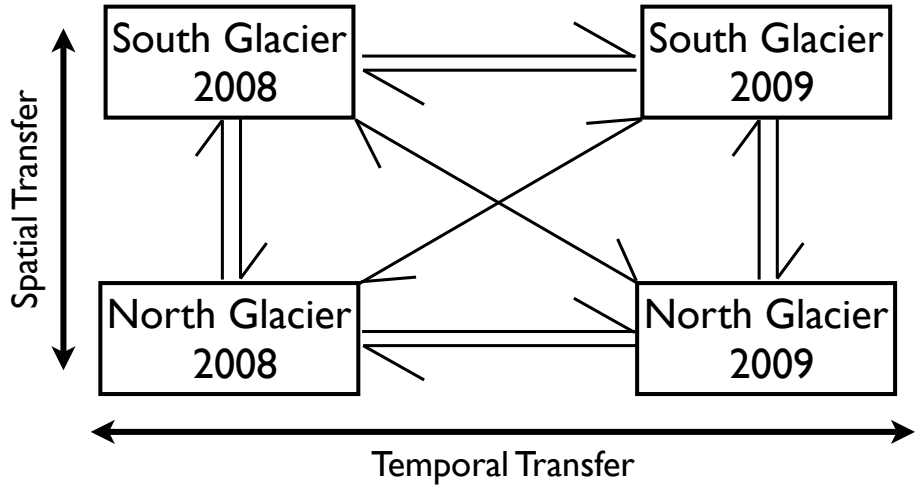

Fig. 2. Diagram of transferability tests. Arrows indicate the possible spatial and temporal transfer of parameter values between data sets.

TCD
4, 2143–2167, 2010

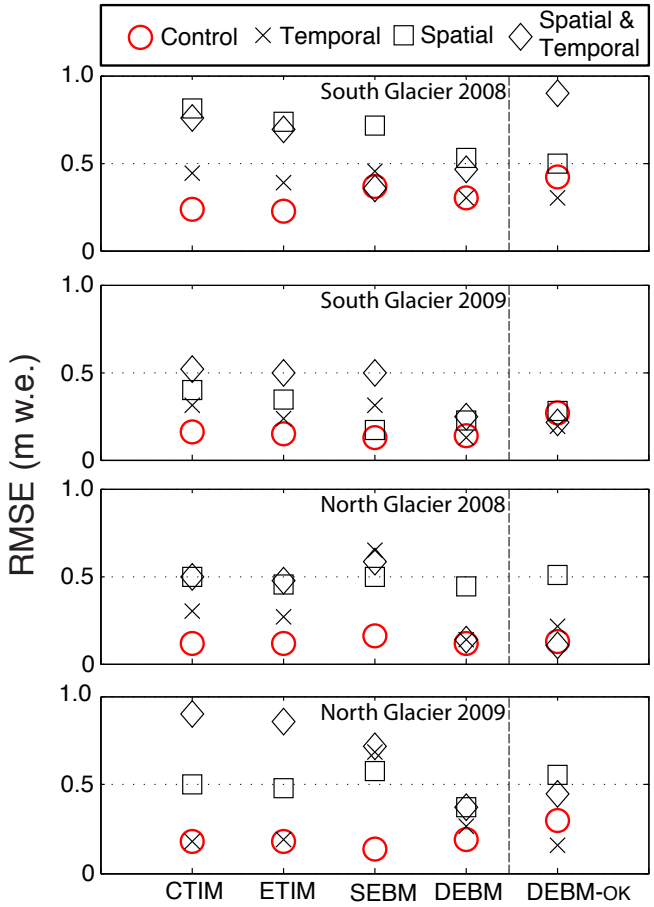

Fig. 3. RMSE for the control runs and the parameter transfer tests for each of the four melt models. Each panel represents one data set as labelled. DEBM-OK is an adapted version of the DEBM which uses the albedo parameterization of Oerlemans and Knap (1998).

TCD
4, 2143–2167, 2010

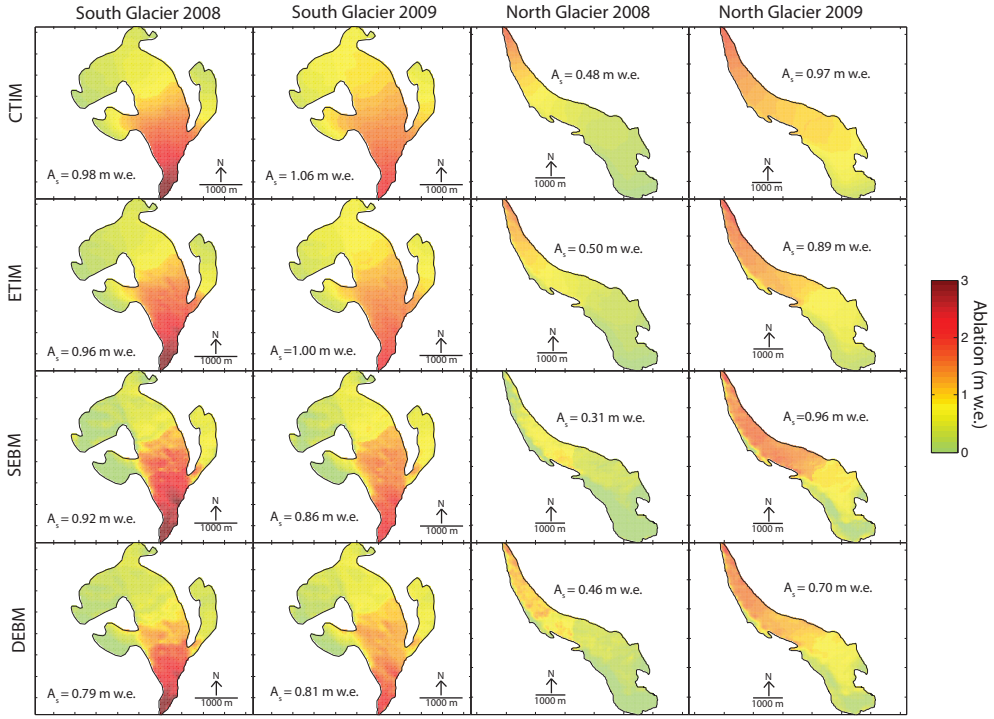

Fig. 4. Distributed surface ablation simulated in the control run by each model for each glacier and year. Simulated glacier-wide surface ablation A_s is recorded in each panel.

TCD
4, 2143–2167, 2010

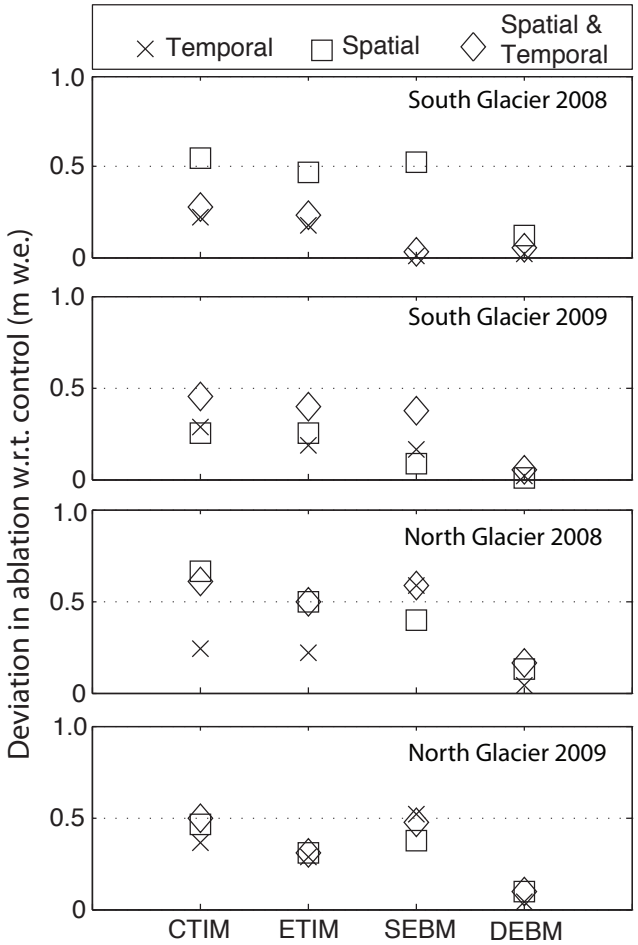

Fig. 5. Deviation between glacier-wide surface ablation estimated in each transfer test and glacier-wide surface ablation estimated in the control run for each model.

TCD
4, 2143–2167, 2010

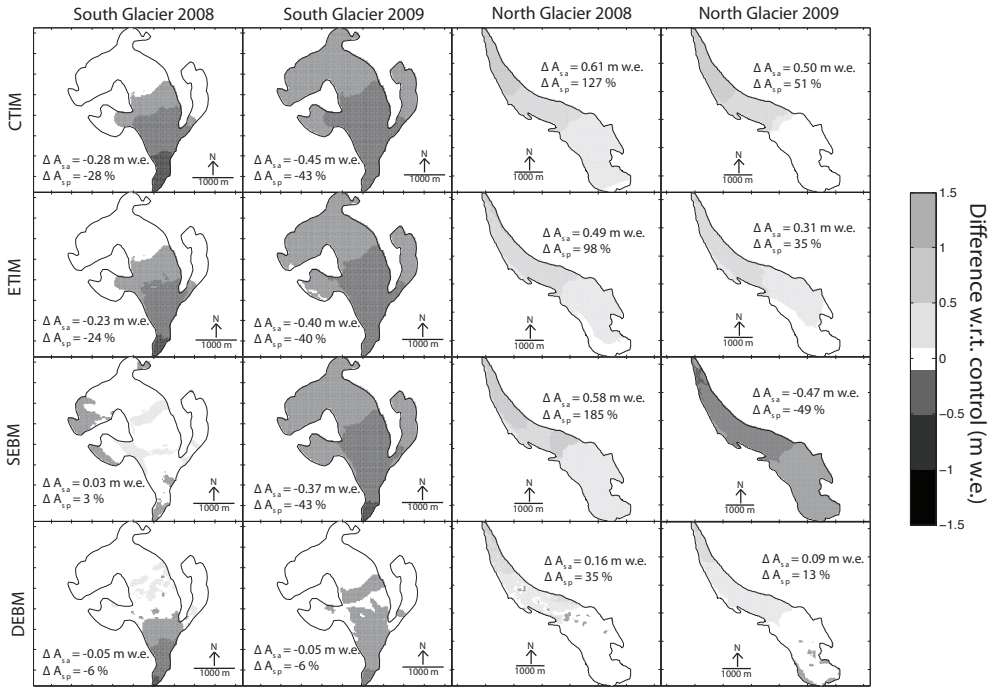

Fig. 6. Difference in surface ablation simulated in the spatial-temporal transfer test and the control run by each model for each glacier and year. ΔA_{sa} is the absolute difference in estimated glacier-wide surface ablation, ΔA_{sp} is the relative difference in estimated glacier-wide surface ablation expressed as a percent.

TCD
4, 2143–2167, 2010